Proceedings of the 5th International Conference on Materials Chemistry and Environmental Engineering
DOI: 10.54254/2755-2721/2025.23606

Recent Advances in Transition Metal Sulfide Bifunctional Electrocatalysts for Overall Water Splitting

Pinyi Chen

Xiamen University, Xiamen, China
37420222204291@stu.xmu.edu.cn

Abstract: In response to the increasingly severe energy crisis and environmental pollution, electrocatalytic hydrogen production has been considered an ideal alternative to fossil fuels because of its sustainability, abundance, and zero emissions. Electrocatalytic water splitting includes two parts, the oxygen evolution reaction (OER) and hydrogen evolution reaction (HER), and high-quality bifunctional electrocatalysts can avoid cross-effects between electrodes, simplify electrolyzer design, and reduce costs. Among them, transition metal sulfides (TMS) possess unique electronic orbital structures, two-dimensional characteristics, low cost, tunable electronic properties, and abundant active sites, showing great potential. This review introduces the HER/OER mechanisms in electrocatalytic water splitting and discusses key electrochemical parameters used to evaluate HER/OER performance. We systematically review the synthesis methods of three representative transition metal sulfide bifunctional catalysts, including hydrothermal, solvothermal, and electrodeposition methods, and summarize the strategies to improve catalyst performance by adjusting microstructure and electronic properties, with a focus on the structure-function relationship of the catalysts.

Keywords: Overall Water Splitting, Transition Metal Sulfides, Bifunctional Electrocatalysts, Hydrogen Energy

1. Introduction

The global tension between economic development and environmental protection has intensified. Fossil fuels, like coal, oil, and natural gas, were excessively consumed, which led to a environmental pollution and severe energy crisis, including the greenhouse effect [1]. Although solar, tidal, and wind energies are widely available and sustainable, they face challenges such as being affected by various natural conditions and economic constraints, making it difficult to meet large-scale, continuous power supply needs [2]. In contrast, hydrogen, widely recognized as a "green energy," holds great potential. A series of large-scale hydrogen production technologies have been developed, such as coal gasification, biogas reforming, and water electrolysis [3-5]. Among them, electrochemical water splitting (EWS) offers zero emissions, lower production costs, and higher purity, making it an ideal choice.

Electrocatalytic water splitting involves the HER and OER. To avoid harmful cross-effects between electrodes prepared with different electrocatalysts, simplify electrolyzer design, and reduce overall manufacturing costs, researchers are striving to develop high-quality bifunctional electrocatalysts that efficiently produce both hydrogen and oxygen, or modify existing HER or OER electrocatalysts to possess bifunctional properties. Over the past five years, the number of

© 2025 The Authors. This is an open access article distributed under the terms of the Creative Commons Attribution License 4.0 (https://creativecommons.org/licenses/by/4.0/).

DOI: 10.54254/2755-2721/2025.23606

publications on overall water splitting (OWS) has dramatically increased [6]. In general, to produce gas products, the minimum voltage required is 1.23 V. However, HER and OER are two-electron and four-electron-proton transfer reactions, respectively, which create significant energy barriers in terms of kinetics. Additionally, the contact between the electrolyzer electrodes introduces other unavoidable obstacles, severely impacting the performance of OWS. In practice, the water splitting voltage is much higher than the theoretical value. Consequently, researchers have been making efforts to develop efficient and steady bifunctional electrocatalysts for OWS to enhance the overall system efficiency. While noble metals and their oxides exhibit excellent performance, their low abundance and high cost constraint large-scale applications. In this regard, transition metal-based electrocatalysts can serve as a good alternative.

Transition metal sulfides (TMS) have attracted global research interest, considering their unique electronic orbital structures, two-dimensional characteristics, low cost, tunable electronic properties, and abundant active sites. Compared to metal-oxide bonds, the metal-sulfide ionic bond in TMS is weaker, which enhances electrical conductivity and reduces catalytic kinetic barriers for electrocatalytic water splitting, thereby improving performance. TMS compounds, such as FeS, NiS, WS_2, CoS_2 and MoS_2, have shown great potential in numerous energy-related applications, especially in electrocatalysis, photocatalysis, and metal-air batteries [7-11].

This paper introduces the mechanism of OWS, discusses the synthesis methods of several transition metal sulfide bifunctional catalysts, and briefly outlines the relation between structure of TMS electrocatalysts and their performance in OWS electrocatalysis.

2. Hydrogen evolution and Oxygen Evolution Reaction mechanisms

Two key half-cell reactions are involved in EWS: the HER and the OER, the former of which occurs at the cathode while the latter occurs at the anode. During electrode reactions, to overcome the thermodynamic energy barrier, a higher voltage than thermodynamic calculation results is required, and this difference is called overpotential (η). Thus, the actual potentials for the two water splitting half-reactions can be expressed as [12]:

$$E_{HER} = E^0_{HER} + iR + \eta_{HER}$$

$$E_{OER} = E^0_{OER} + iR + \eta_{OER}$$

where iR represents the system ohmic potential drop, η is the overpotential, E^0_{HER}=0 and E^0_{OER}=1.23 V. Overpotential (η) is commonly used to characterize the activity of electrocatalytic materials: a smaller overpotential indicates the reaction occurs more readily. The rate-determining step (RDS) is an effective pathway to lower the reaction overpotential. Therefore, to prepare effective electrocatalysts, it is essential to understand the mechanisms of both HER and OER.

2.1. Hydrogen Evolution Reaction (HER)

HER is relatively simpler compared to OER, involving only two electron transfers and one intermediate (H^*) [13]. The HER mechanism consists of three steps, there are: First step - Volmer, Second step - Heyrovsky, and Third step - Tafel. In acidic and alkaline media, the HER mechanism hardly differs, but with different proton sources. In acidic conditions, the proton source is H_3O^+, while in alkaline conditions, it is H_2O. This multi-step basic mechanism of the reaction is commonly referred to as the Volmer-Heyrovsky mechanism or Volmer-Tafel mechanism, which is shown below:

In acidic solution:

$$\text{First step: } H_3O^+ + e^- + * \rightarrow H^* + H_2O(l) \quad (1)$$

DOI: 10.54254/2755-2721/2025.23606

$$\text{Second step: } H^* + H^* \rightarrow H_2(g) + 2^* \quad (2)$$

$$\text{Third step: } H^* + H_3O^+ + e^- + \rightarrow H_2(g) + H_2O(l) \quad (3)$$

In neutral and alkaline solution:

$$\text{First step: } H_2O\ (l) + e^- + * \rightarrow H^* + OH^-\ (aq) \quad (4)$$

$$\text{Second step: } H_2O(l) + e^- + H^* \rightarrow H_2(g) + OH^-(aq) \quad (5)$$

$$\text{Third step: } H^* + H^* \rightarrow H_2(g) + 2^* \quad (6)$$

where * represents an active site, so, naturally, a hydrogen atom bound to it is indicated as H^*.

The Volmer reaction occurs during the first step of HER, where protons accept electrons and are adsorbed on the electrode surface, forming hydrogen atoms (H^*). Subsequently, to form hydrogen molecules, H^* undergoes desorption through two different ways: one is the Heyrovsky reaction, where to produce hydrogen gas, adsorbed hydrogen atoms combine with protons from the electrolyte. The other pathway, where adsorbed on the catalyst in advance, hydrogen atoms combine with each other to form molecules, is referred to as the Tafel reaction desorption. The HER mechanism in acidic and alkaline solutions is shown in Figure 1. It can be observed that the key steps in hydrogen evolution are the transfer of electrons and the desorption of hydrogen atoms, with the slow reaction in these two steps being the rate-determining step of hydrogen evolution. Practically, by measuring the magnitude of the Tafel slope, the HER reaction kinetics can be determined.

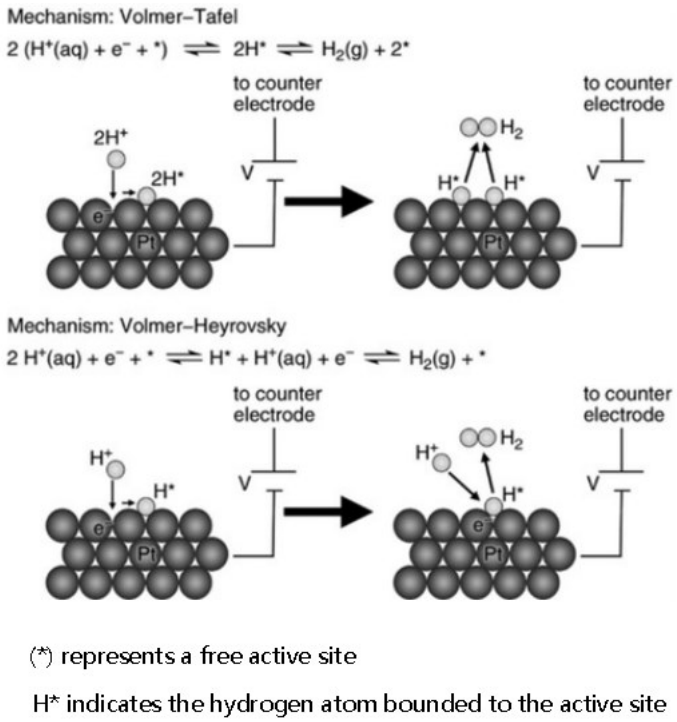


Figure 1: HER mechanisms [13]

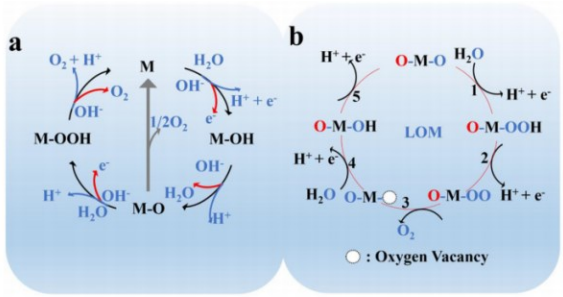
2.2. Oxygen Evolution Reaction (OER)

The OER is a four-proton coupled electron transfer reaction with relatively complex reaction processes, involving three different intermediates (O^*, OH^*, OOH^*). The adsorbate evolution mechanism (AEM) and the lattice oxygen mechanism (LOM) are two currently accepted OER mechanisms [14].

DOI: 10.54254/2755-2721/2025.23606

Figure 2a shows the widely recognised AEM reaction pathway for different solutions. After OH/H_2O is adsorbed, electron transfer occurs to form the OH^* intermediate. OH^* undergoes deprotonation followed by another electron transfer, forming O^* intermediate and OOH^* intermediate; The OOH^* intermediate then undergoes deprotonation, resulting in O_2 evolution.

Figure 2b shows the reaction pathway of LOM. LOM is only suitable for reactions in acidic media. Here, an oxygen vacancy is represented as V_o.



(a). AEM in acidic (blue line) and alkaline (red line) solutions (b). LOM in acidic solutions

Figure 2: Diagram of OER mechanisms [14]

In acidic solution (AEM):

$$H_2O \rightarrow OH^* + H^+ + e^- \quad (7)$$

$$OH^* \rightarrow O^* + H^+ + e^- \quad (8)$$

$$O^* + H_2O \rightarrow OOH^* + H+ + e^- \quad (9)$$

$$OOH^* \rightarrow O_2 + H^+ + e^- \quad (10)$$

In acidic solution (LOM):

$$H_2O + O^* \rightarrow OOH^* + H^+ + e^- \quad (11)$$

$$OOH^* \rightarrow OO^* + H^+ + e^- \quad (12)$$

$$OO^* \rightarrow O_2 + OH^* + V_o \quad (13)$$

$$V_o + H_2O \rightarrow OH^* + H^+ + e^- \quad (14)$$

$$OH^* \rightarrow O^* + H^+ + e^- \quad (15)$$

In neutral and alkaline solution (AEM):

$$OH \rightarrow OH^* + e^- \quad (16)$$

$$OH^* + OH \rightarrow O^* + H_2O + e^- \quad (17)$$

$$O^* + OH \rightarrow OOH^* + e^- \quad (18)$$

$$OOH^* + OH \rightarrow O_2 + H_2O + e^- \quad (19)$$

Due to its complexity, the OER reaction rate is extremely slow and has a high overpotential, making it the rate-determining reaction for OWS. The catalyst's activity is dramatically influenced by oxygen intermediates' (OH^*, O^*, OOH^*) surface adsorption-desorption capability. Similar to HER, only catalysts with moderate binding strength are needed. The distribution of the oxygen intermediates (O^*, OH^*, and OOH^*) also significantly affects catalytic performance. The Tafel slope is still used to evaluate catalyst performance, while the free energy difference between OOH^* and OH^*($\Delta G=\Delta G_{OOH*}-\Delta G_{OH*}$) is also thought as a standard to measure catalyst OER performance.

DOI: 10.54254/2755-2721/2025.23606

3. The synthesis of transition metal sulfide bifunctional catalysts

In recent years, benefiting from the rapid development of various technologies and increasingly deeper understanding of bifunctional catalysts, multiple methods have been employed to synthesize different electrocatalysts. The main types of these methods are as follows:

3.1. Hydrothermal method

Compared to other processes, the hydrothermal method is simple and widely applicable. It typically involves synthesizing sulfide electrocatalysts through hydrothermal treatment of solutions containing sulfur sources and metal salt precursors.

Gautam et al. designed POM@ZnCoS NWs on three-dimensional sponge substrate using a two-step simple hydrothermal method [15]. In the second hydrothermal reaction step, through ion exchange reaction between ZnCo binary oxide nanowire precursor and Na_2S, ZnCoS nanowires were synthesized. POM@ZnCoS NWs were obtained by anchoring PW_{12} nanoparticles on the nanowire surface. The anchoring led to relatively low electron transfer resistance and provided additional active sites; the special morphological characteristics and nanowires also provided many uncovered active sites, increased ion diffusion rate and reduced diffusion path distance, thus achieving effective charge transfer. Meanwhile, a large number of high-spin Co^{3+} ions could effectively contribute to the catalyst's activity for reactions on both electrodes. These factors enabled the synthesized POM@ZnCoS NWs to perform well. For HER, the apparent Tafel slope of POM@ZnCoS/NF material was 53.5 mV dec^{-1}. To reach current densities of 10 and 40 mA cm^{-2}, compared with ZnCo DHNWs (227/363 mV), ZnCoS NWs (206/357 mV) and POM/NF (240/369 mV), POM@ZnCoS NWs required overpotentials of 170 and 337 mV respectively, even superior to commercial Pt/C catalyst's overpotential (184/479 mV), indicating its more excellent HER behavior. At the anode (OER), to reach current densities of 20 and 50 mA cm^{-2}, the overpotentials POM@ZnCoS/NF shown were 200 and 300 mV, superior to ZnCo DHNWs, whose overpotentials shown were 200/430 mV, ZnCoS NWs (240/400 mV), and RuO_2 (260/430 mV) (Figure 3a). The apparent Tafel slope was 67.7 mV dec^{-1} for POM@ZnCoS/NF material (Figure 3b).

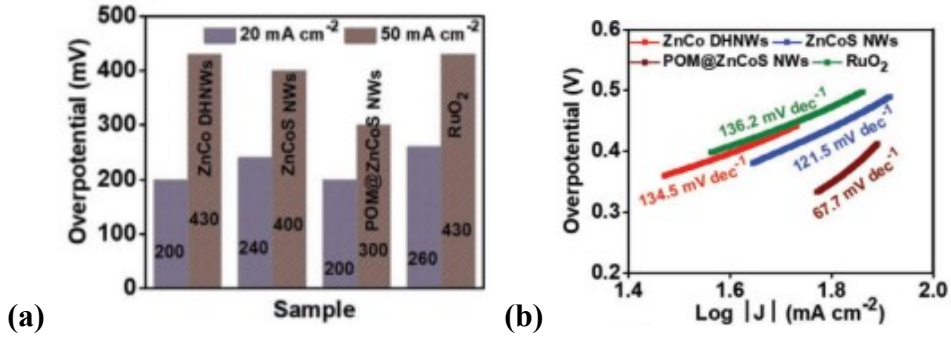


Figure 3: Comparison of a) overpotentials at a scanning rate of 10 mV s^{-1}, b) Tafel curves of ZnCo DHNWs, ZnCoS NWs, POM@ZnCoS/NF, and RuO_2 electrocatalysts for O_2 evolution activity measurement [15]

3.2. Solvothermal method

The solvothermal method dissolves precursors in non-aqueous solvents to form a uniform solution. Through heating and applied pressure, it promotes the dissolution and reaction of reactants. Compared to the hydrothermal method, the solvothermal method can adjust the physical and chemical properties

DOI: 10.54254/2755-2721/2025.23606

of the reaction environment, offering greater flexibility in controlling catalyst morphology, particle size, and crystal structure, thus helping to optimize catalytic performance.

Zhang et al. used the in-situ solvothermal method, with $FeCl_3 \cdot 6H_2O$ and $SnCl_2 \cdot 2H_2O$ as metal sources and thioacetamide as sulfur source, to synthesize heterojunction catalyst $SnFeS_xO_y$/NF [16]. For HER, to reach 10 mA cm^{-2} in N_2 saturated 1 M KOH, the overpotential $SnFeS_xO_y$/NF required was 85 mV, lower than SnS_xO_y/NF(98 mV), $SnFeO_x$/NF(178 mV), and FeS_xO_y/NF(204 mV). Moreover, $SnFeS_xO_y$/NF's Tafel slope was 90 mV dec^{-1}, lower than SnS_xO_y/NF, FeS_xO_y/NF, and $SnFeO_x$/NF, indicating good HER kinetics. For OER, to reach a current density of 100 mA cm^{-2} , $SnFeS_xO_y$/NF needed an over-potential of only 281 mV, superior to SnS_xO_y/NF, FeS_xO_y/NF, $SnFeO_x$/NF, commercial IrO_2 (398 mV) and most sulfides and oxides. $SnFeS_xO_y$/NF's Tafel slope was 60 mV dec^{-1}, while the Tafel slope of $SnFeO_x$/NF, FeS_xO_y/NF and SnS_xO_y/NF were 73 mV dec^{-1}, 75 mV dec^{-1} and 90 mV dec^{-1} respectively. The measured electrochemically active surface area (ECSA) data showed that $SnFeS_xO_y$/NF's ECSA was higher than SnS_xO_y/NF, FeS_xO_y/NF, and $SnFeO_x$/NF, indicating more active sites. The acceleration of electron transfer was attributed to the formation of Sn/Fe sulfide/oxide heterojunctions and the synergistic effect between Sn and Fe sites, which resulted in the OER energy barrier reduction, and thus improving catalytic performance.

Similarly, Zhang et al. prepared Ni_3S_2-MoS_x/NF using a modified one-step solvothermal method [17]. While Ni foam showed inherent HER catalytic activity, Ni_3S_2-MoS_x/NF exhibited outstanding HER performance. The onset potential of -14 mV (1 mA cm^{-2}) it required was low, very close to 50 wt% Pt/C/NF (-8 mV). In comparison, the HER activity of Ni_3S_2-MoS_x/NF (w) nanosheets is lower than Ni_3S_2-MoS_x/NF nanowires. At a overpotential of only 65 mV, the Ni_3S_2-MoS_x/NF composite material achieved 10 mA cm^{-2}, superior to 100 mV for Ni_3Se_2/Cu foam, 110 mV for MoS_2/Ni_3S_2 heterojunction, 127 mV for Ni_3S_2-MoS_x/NF(w), etc. Ni_3S_2-MoS_x/NF's Tafel slope was 81 mV dec^{-1}, higher than 48 mV dec^{-1} for Pt/C/NF but better than Ni_3S_2-MoS_x/NF(w) (129 mV dec^{-1}) and bare Ni foam (155 mV dec^{-1}). For OER, to provide 50 mA cm^{-2} , the Ni_3S_2-MoS_x/NF catalyst required an overpotential of 312 mV, showing relatively good performance compared to reported nickel-based catalysts, such as NiS/Ni foam which required 335 mV at the same current density. Ni_3S_2-MoS_x/NF's Tafel slope was 103 mV dec^{-1}, lower than 138 mV dec^{-1} for Ni_3S_2-MoS_x/NF(w) and 142 mV dec^{-1} for Ni foam, indicating effective catalytic reaction kinetics. High-resolution transmission electron microscopy (HRTEM) images (Figure 4) revealed that Ni_3S_2-MoS_x nanowires possessed a short-range order structure with abundant defects. The large number of defect sites in Ni_3S_2-MoS_x could potentially activate catalytic active sites, cause catalytic interface cracking, accelerate OH/H_2O molecular adsorption, and promote water splitting.

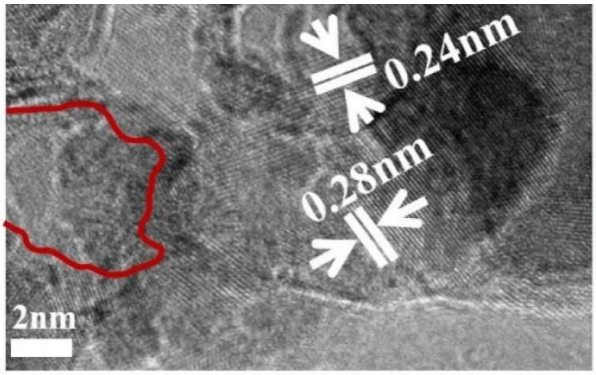


Figure 4: HRTEM image of Ni_3S_2-MoS_x nanorods. The red curve marked the amorphous domain, ascribed to amorphous MoS_x [17]

DOI: 10.54254/2755-2721/2025.23606

3.3. Electrodeposition

While hydrothermal or solvothermal methods are commonly used to synthesize TMS, these processes require high temperature, high energy etching conditions, and are time-consuming. In comparison, electrodeposition is easy, cost-effective, and capable of fabricating large surface area structures, making it an ideal method for producing many electrocatalysts. Its principle is based on the redox reactions of positive and negative ions in electrolyte solutions under external electric field, with electrons undergoing oxidation-reduction reactions at the electrode to form an electroplated layer.

For example, Meng et al. used in-situ electrodeposition technology, immersing NF in a mixed solution of 0.5 M $FeSO_4 \cdot 7H_2O$, 0.5 M $Ni(NO_3)_2 \cdot 6H_2O$, 1.0 M KCl, and 1.0 M $Na_2S_2O_3 \cdot 5H_2O$ for 5 minutes of deposition, directly preparing NiFeS/NF bifunctional electrocatalyst [18]. They used cyclic voltammetry (CV) to measure its double-layer capacitance at scanning speeds varying from 20 to 120 mV s^{-1}. For HER, under 1.0 M KOH conditions at 10 mA cm^{-2}, NiFeS/NF required an overpotential of 75 mV, lower than 279 mV for NiFe-LDH/NF, 124 mV for NiS/NF, and 149 mV for FeS/NF. The Tafel slope for NiFeS/NF is 60.23 mV dec^{-1}, which is also the smallest of the four mentioned above. For OER, compared to single-component catalysts FeS/NF and NiS/NF, NiFeS/NF showed significantly improved performance. NiFeS/NF's overpotential at 10 mA cm^{-2} was 210 mV, superior to FeS/NF (224 mV), NiS/NF (260 mV), and NiFe-LDH/NF (234 mV). NiFeS/NF's Tafel slope was approximately 40.9 mV dec^{-1}, also superior to FeS/NF, NiS/NF, NiFe-LDH/NF, RuO_2, whose corresponding slopes were 47 mV dec^{-1}, 62.9 mV dec^{-1}, 53.4 mV dec^{-1}, and 108.7 mV dec^{-1}. SEM images (Figure 5) and TEM images (Figure 6) showed that NiFeS/NF's microstructure exhibited ordered nanoscale sheet-like morphology, providing numerous active sites for electron transfer; additionally, its good crystallinity offered higher electron transfer efficiency than amorphous phases, thus enabling NiFeS/NF to demonstrate excellent electrocatalytic water splitting performance.

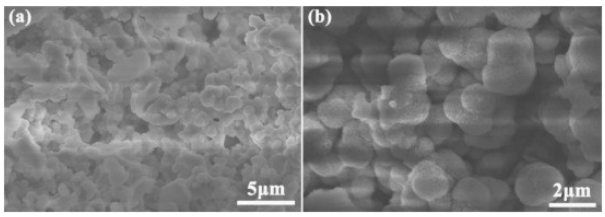
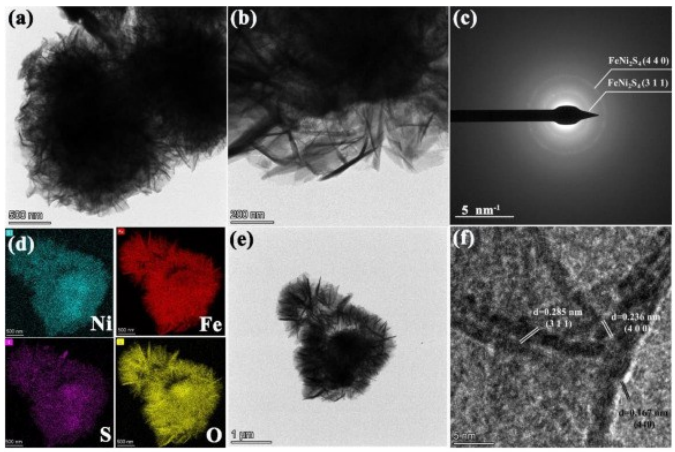


Figure 5: SEM images of NiFeS/NF with different magnification [18]



(a,b,e) Low magnification TEM images;
(c) SAED analysis; (e) EDS element mapping images;
(f) HRTEM images

Figure 6: TEM images [18]

DOI: 10.54254/2755-2721/2025.23606

Li et al. used the Ultrafast Pulse Electrodeposition (UPED) method to first obtain zinc-doped nickel sulfide with polyhedron hollow nanospheres (ZnCoNiS/PHS/CP) as a bifunctional catalyst for OWS with highly efficiency and stability in neutral media [19]. The optimized Zn_{10}-CoNiS possessed semi-rich active sites and, through appropriate Zn doping, demonstrated excellent stability and desirable catalytic activity. Using a typical three-electrode system with commercial Pt/C catalyst as the working electrode for comparison, LSV tests were conducted in 1 M PBS at a scanning speed of 2 mV s^{-1}, obtaining polarization curves for Zn-CoNiS catalyst, undoped CoNiS catalyst, and Pt/C catalyst. Zn_{10}-CoNiS's overpotential was 213 mV, superior to Zn_5-CoNiS (286 mV), Zn_{15}-CoNiS (226 mV), and Zn_{20}-CoNiS (267 mV), which is lowest among these and also superior to CoNiS (256 mV). Moreover, Zn_{10}-CoNiS's Tafel slope (126 mV dec^{-1}) is smaller compared to Zn_5-CoNiS (176 mV dec^{-1}), Zn_{15}-CoNiS (142 mV dec^{-1}), Zn_{20}-CoNiS (151 mV dec^{-1}), and CoNiS (157 mV dec^{-1}) , and close to Pt/C electrodes (122 mV dec^{-1}). Specifically, among the five TMS-based catalysts, Zn_{10}-CoNiS demonstrated the fastest HER kinetics. For OER, to reach 10 mA cm^{-2}, Zn_{10}-CoNiS required an overpotential of 414 mV, significantly lower than other catalysts. In comparison, Zn_5-CoNiS, Zn_{15}-CoNiS, Zn_{20}-CoNiS, and CoNiS required 588, 456, 547, and 604 mV respectively. In neutral media, the Tafel slopes for Zn_5-CoNiS, Zn_{10}-CoNiS, Zn_{15}-CoNiS, Zn_{20}-CoNiS, and CoNiS were 191, 131, 158, 167, and 231 mV dec^{-1} respectively. The superior performance of Zn_{10}-CoNiS was attributed to the zinc doping effect introducing more active sites and optimizing the electronic structure.

4. Conclusion

This paper discusses transition metal sulfide bifunctional catalysts prepared by three methods. To reach a current density of 10 mA cm^{-2}, the two-step simple hydrothermal method produced POM@ZnCoS NWs with an HER overpotential of 170 mV and Tafel slope of 53.5 mV dec^{-1}; the in-situ solvothermal method produced heterojunction catalyst $SnFeS_xO_y$/NF with an HER overpotential of 85 mV and Tafel slope of 90 mV dec^{-1}; the modified one-step solvothermal method produced Ni_3S_2-MoS_x/NF with an HER overpotential of 65 mV and Tafel slope of 81 mV dec^{-1}; and the in-situ electrodeposition technique produced NiFeS/NF bifunctional catalyst with an HER overpotential of 75 mV and Tafel slope of 60.23 mV dec^{-1}. Comparing these data shows that catalysts obtained through the two-step simple hydrothermal method have the highest HER overpotential, making catalytic reactions more difficult; catalysts prepared using the modified one-step solvothermal method have the lowest HER overpotential, facilitating easier catalytic reactions; catalysts prepared using in-situ electrodeposition technology not only have relatively low overpotential but also lower Tafel slopes, showing superior performance. The improved one-step solvothermal method compared to hydrothermal method can adjust the reaction environment's physical and chemical properties, effectively controlling catalyst structure, resulting in catalysts with more active sites and lower energy barriers, thus having excellent performance. The in-situ electrodeposition technique applies an external electric field, forming an electroplated layer through electrode surface oxidation-reduction reactions, enabling catalysts to exhibit ordered microstructure and good crystallinity, providing numerous active sites while maintaining high electron transfer efficiency, thus demonstrating outstanding electrocatalytic water splitting performance. Overall, these synthesized catalysts all demonstrate relatively superior performance, mainly benefiting from: 1) Their unique structures, such as interfaces, defects, vacancies, etc., introducing rich active sites; 2) Changes in electronic configuration; 3) Synergistic effects between different metals.

References

[1] *Askarniya, Z.; Sun, X.; Wang, Z.; et al. (2023). Cavitation-based technologies for pretreatment and processing of food wastes: Major applications and mechanisms – A review. Chemical Engineering Journal. 454. 140388. doi: 10.1016/j.cej.2022.140388.*

DOI: 10.54254/2755-2721/2025.23606

[2] Jacobson, M. Z.; Delucchi, M. A.; Bauer, Z. A. F.; et al. (2017). 100% Clean and Renewable Wind, Water, and Sunlight All-Sector Energy Roadmaps for 139 Countries of the World. Joule. 1. doi: 10.1016/j.joule.2017.07.005.
[3] Midilli, A.; Kucuk, H.; Topal, M. E.; et al. (2021). A comprehensive review on hydrogen production from co al gasification: Challenges and Opportunities. International Journal of Hydrogen Energy. 46. doi: 10.1016/j. ijhydene.2021.05.088.
[4] Kumar, R.; Kumar, A.; Pal, A. (2022). Overview of hydrogen production from biogas reforming: Technological advancement. International Journal of Hydrogen Energy. 47. doi: 10.1016/j.ijhydene.2022.08.059.
[5] Wang, K.; Huang, J.; Chen, H.; et al. Recent Progress in High Entropy Alloys for Electrocatalysts[J]. Electrochemical Energy Reviews, 2022, 5(S1): 17. doi: 10.1007/s41918-022-00144-88.
[6] Wang, C.; Guo, W.; Chen, T.; et al. (2024). Advanced noble-metal/transition-metal/metal-free electrocatalysts for hydrogen evolution reaction in water-electrolysis for hydrogen production. Coordination Chemistry Reviews. 514. 215899. doi: 10.1016/j.ccr.2024.215899.
[7] Mei, J.; Deng, Y.; Cheng, X.; et al. (2023). Recent advances in iron-based sulfides electrocatalysts for oxygen and hydrogen evolution reaction. Chinese Chemical Letters. 35. 108900. doi: 10.1016/j.cclet.2023.108900.
[8] Schalenbach, M.; Kasian, O.; Mayrhofer, K. J. J. (2018). An alkaline water electrolyzer with nickel electrod es enables efficient high current density operation. International Journal of Hydrogen Energy. 43. doi: 10.1 016/j.ijhydene.2018.04.219.
[9] Sobczynski, A.; Yildiz, A.; Bard, A. J.; et al. (1988). Tungsten disulfide: a novel hydrogen evolution catalyst for water decomposition. The Journal of Physical Chemistry, 92, 2311-2315. doi: 10.1021/J100319A042.
[10] Zhang, J.; Liu, Y.; Sun, C.; et al. (2018). Accelerated Hydrogen Evolution Reaction in CoS2 by Transition-Metal Doping. ACS Energy Letters. 3. doi: 10.1021/acsenergylett.8b00066.
[11] Fu, Y.-G.; Liu, H.-Q.; Liu, C.; et al. (2023). Ultralight porous carbon loaded Co-doped MoS2 as an efficient electrocatalyst for hydrogen evolution reaction in acidic and alkaline media. Journal of Alloys and Compounds. 967. 171748. doi: 10.1016/j.jallcom.2023.171748.
[12] Zhang, W.; Cui, L.; Liu, J. (2019). Recent advances in cobalt-based electrocatalysts for hydrogen and oxygen evolution reactions. Journal of Alloys and Compounds. 821. 153542. doi: 10.1016/j.jallcom.2019.153542.
[13] Li, A.; Sun, Y.; Yao, T.; et al. (2018). Earth-Abundant Transition-Metal Based Electrocatalysts for Water Electrolysis to Produce Renewable Hydrogen. Chemistry. 24. doi: 10.1002/chem.201803749.
[14] Zhang, Y., Jiang, Y., Abdukayum, A., Xie, X., Gao, S., Liu, X., Zhang, L., Liu, Q., & Hu, G. (2024). Recent advances in selenide-based electrocatalysts for hydrogen/oxygen evolution reaction: From mechanism and synthesis to application. Materials Today Energy. doi: 10.1016/j.mtener.2024.101641
[15] Gautam, J.; Liu, Y.; Gu, J.; et al. Fabrication of Polyoxometalate Anchored Zinc Cobalt Sulfide Nanowires as a Remarkable Bifunctional Electrocatalyst for Overall Water Splitting. Adv. Funct. Mater. 2021, 31, 2106147. doi: 10.1002/adfm.202106147.
[16] Zhang, T.; Han, J.; Tang, T.; et al. (2022). Binder-free bifunctional SnFe sulfide/oxyhydroxide heterostructur e electrocatalysts for overall water splitting. International Journal of Hydrogen Energy. 48. doi: 10.1016/j.ij hydene.2022.11.039.
[17] Zhang, D.; Jiang, L.; Liu, Y.; et al. (2019). Ni3S2-MoSx nanorods grown on Ni foam as high-efficient electr ocatalysts for overall water splitting. International Journal of Hydrogen Energy. 44. 17900-17908. doi: 10.1 016/j.ijhydene.2019.05.157.
[18] Meng, L.; Xuan, H.; Wang, J.; et al. (2023). One-step electrodeposition synthesis of bimetallic sulfides for h ighly efficient electrocatalytic water splitting. International Journal of Hydrogen Energy. 51. doi: 10.1016/j.i jhydene.2023.08.143.
[19] Li, X.; Yan, W.; Fan, B.; et al. (2024). In situ electrodeposited Zn-doped CoNiS as an efficient and stable electrocatalyst for overall water splitting in neutral media. Colloids and Surfaces A: Physicochemical and Engineering Aspects. 694. 134176. doi: 10.1016/j.colsurfa.2024.134176.